

PAPER

Questioning liquid droplet stability on nanowire tips: from theory to experiment

To cite this article: Lea Ghisalberti *et al* 2019 *Nanotechnology* **30** 285604

View the [article online](#) for updates and enhancements.




IOP | ebooks™

Bringing you innovative digital publishing with leading voices to create your essential collection of books in STEM research.

Start exploring the collection - download the first chapter of every title for free.

Questioning liquid droplet stability on nanowire tips: from theory to experiment

Lea Ghisalberti¹, Heidi Potts¹, Martin Friedl¹, Mahdi Zamani¹,
Lucas Güniat¹, Gözde Tütüncüoğlu¹, W Craig Carter^{1,2} and
Anna Fontcuberta i Morral^{1,3} 

¹Laboratoire des Matériaux Semiconducteurs, Institut des Matériaux, Ecole Polytechnique Fédérale de Lausanne, 1015 Lausanne, Switzerland

²Department of Materials Science and Engineering, MIT, Cambridge, MA, United States of America

E-mail: anna.fontcuberta-morral@epfl.ch

Received 20 January 2019, revised 25 March 2019

Accepted for publication 26 March 2019

Published 25 April 2019



CrossMark

Abstract

Liquid droplets sitting on nanowire (NW) tips constitute the starting point of the vapor–liquid–solid method of NW growth. Shape and volume of the droplet have been linked to a variety of growth phenomena ranging from the modification of growth direction, NW orientation, crystal phase, and even polarity. In this work we focus on numerical and theoretical analysis of the stability of liquid droplets on NW tips, explaining the peculiarity of this condition with respect to the wetting of planar surfaces. We highlight the role of droplet pinning at the tip in engineering the contact angle. Experimental results on the characteristics of In droplets of variable volume sitting on the tips or side facets of InAs NWs are also provided. This work contributes to the fundamental understanding of the nature of droplets contact angle at the tip of NWs and to the improvement of the engineering of such nanostructures.

Supplementary material for this article is available [online](#)

Keywords: nanowire, contact angle, stability, tilting, growth direction

(Some figures may appear in colour only in the online journal)

Introduction

Nanowires (NWs) are filamentary crystals with a tailored diameter in the few nanometer range. Semiconductor NWs and in particular III–V NWs, are promising building blocks for next-generation computing, sensing and energy harvesting devices [1–7]. NWs can be obtained in arrays of uniform structures [8–11] as well as by self-assembly on a substrate [12–16]. In this case, the characteristics of the structure may exhibit a higher degree of variation in terms of structure, growth direction and even crystal polarity. Flexibility of NW characteristics in the self-assembled approach may originate from the dispersion in NWs distance, diameter and nucleation points [17–19].

The most common method used for the growth of NWs is the vapor–liquid–solid method, VLS, in which a liquid metal

is used to preferentially decompose and gather growth precursors. Upon supersaturation of the precursors in the liquid phase, a solid NW is formed [20, 21]. Recently, it has been shown that the characteristics of the liquid droplet are essential for many aspect of the growth of the NWs. In particular, it has been shown that the droplet contact angle with the solid NW determines the crystal phase, growth direction, orientation and polarity of the NW itself [8, 22–26]. To that end, we believe that the direct translation of capillarity laws from the planar to the non-planar nanoscale case has not been discussed with enough depth. Important works have been published regarding the possible role of edges [27–29] and the effect of the droplet volume on the contact angle [25, 30]. However, given the prominent role of the contact angle in NW growth, this point deserves clarification. In this paper, we define basic capillarity laws determining the stability of nanoscale droplets on the tip of NWs. We start by providing a theoretical basis from a historical point of view.

³ Author to whom any correspondence should be addressed.

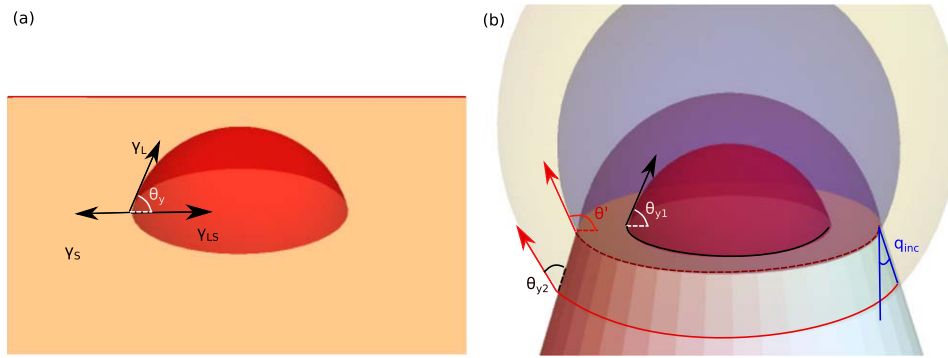


Figure 1. (a) Sketch of a sessile droplet wetting an ideal infinite solid and whose shape is characterized by the equilibrium angle, θ_Y , minimizing the surface energy of the system. (b) Sketch representing the pinning effect characterizing the wetting of variable volume droplets on top of a truncated cone. When the droplet triple phase line (TPL) is in touch with the edge, there is a continuous range of contact angles available from θ_{Y1} and $\theta_{Y2} + q_{incl}$, with q_{incl} representing the inclination of the sidewalls and θ_{Y2} the sidewalls equilibrium angle.

We then follow-up with numerical simulations that explain the stability conditions of the droplet, based on surface energy minimization. Finally, we provide experimental results on the In (droplet)/InAs (NW) system, consistent with the theoretical considerations. Our work provides new insights into the wetting properties of VLS droplets and improves our understanding of this NW growth mechanism.

Theoretical considerations

The Young–Dupré’s equation describes the wetting of a sessile droplet on a flat substrate. It defines the contact angle θ_Y as a balance between adhesion to the surface and the cohesive forces of the droplet constituents. Figure 1(a) shows the typical setting of the equation. γ_S , γ_L and γ_{SL} correspond respectively to the solid–vapor, liquid–vapor and liquid–solid interfacial energies. In the Young–Dupré equation, only the capillary forces in the plane of the solid sum to zero

$$\gamma_S = \gamma_{SL} + \gamma_L \cos \theta_Y. \quad (1)$$

Equation (1) assumes that the atoms in and on the surface of the solid are immobile. The vertical capillary forces are balanced by elastic stresses resolved onto the solid surface, as their sum should be zero everywhere across the contact surface in order to ensure the equilibrium. This equilibrium may change as soon as the surface available to the liquid becomes finite, close to the size of the liquid–solid interface, as is the case at the tip of a NW. A schematic drawing of four possible volume-dependent-scenarios of a liquid droplet wetting a NW tip is shown in figure 1(b). The droplet should change its shape depending on its own volume. Starting at small volumes, the droplet partially wets the tip in a similar manner as on an infinite planar surface (as in figure 1(a)). With the increase of volume, the droplet extends over the NW tip until it gets pinned at the edge. The line defining the interface between the vapor, liquid and solid interface is usually denoted as the triple-phase-line (TPL). The contact angle, θ_{Y1} , defined as the angle between the NW tip surface and the tangent of the droplet at the TPL is equivalent in these two cases. Further volume increase of the droplet results in an

apparent increase in the contact angle and possible wetting on the NW side facets, both in contradiction with the Young–Dupré equation. To date, most of the theoretical analyses of NW growth have considered the literal interpretation of the Young–Dupré equation. In these works, the surface tensions were interpreted by substituting the pinned angle by the Young angle [8, 26, 31–33]. However, the droplet pins as soon as the TPL reaches the edge, thus no conclusions on the solid–liquid interfacial energy can be derived from the contact angle and the values of the other surface energies [34]. In some cases, the equilibrium angle predicted by the Young equation may be satisfied at certain points of the TPL [29]. However, such considerations do not imply that a droplet is in equilibrium. The equilibrium condition is related to the balance of the entire TPL, where all its points satisfy the Young equation. In addition, one should also consider that the droplet surface should exhibit a constant mean curvature to ensure such an equilibrium condition [35]. In practice, there may be more than one solution, some of them representing droplets in a metastable equilibrium. To summarize, the Young–Dupré equation corresponds to a heuristic capillary force balance construction that lacks generality for anything on finite, non-flat surfaces. In general, the solution should correspond to the shape minimizing the total surface energy.

Numerical simulations of sessile droplets on a NW tip

In this section, we provide numerical calculations of the stability of sessile droplets on NW tips as a function of their volume. We also illustrate how the solid–liquid interface evolves as soon as the droplet becomes unstable. The goal of these calculations is to capture the physics behind the wetting of droplets on NW tips. For this, we have simplified the shape of the NW as cylindrical instead of the most commonly observed hexagonal cross-section. Indeed we observed that for droplet wetting the NW’s top, the general tendency is to maintain a spherical-cap shape. For the range of NW diameters considered here, the corners of the hexagonal cross-section do not influence the overall wetting and thus their

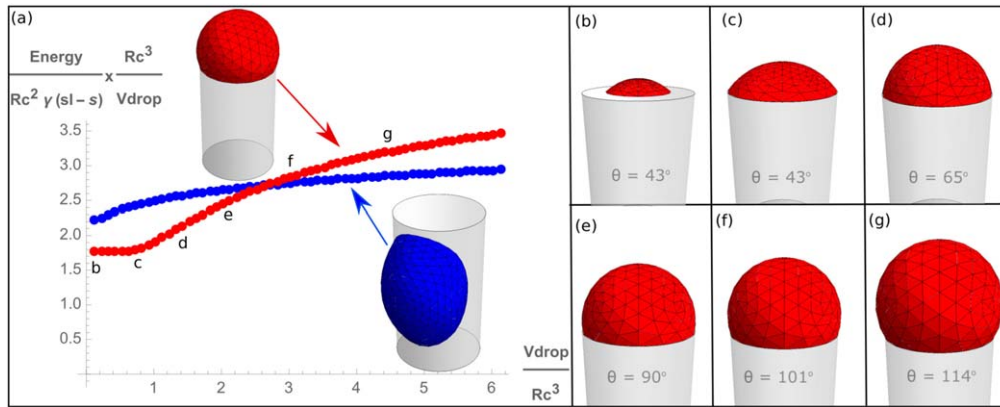


Figure 2. (a) Results of the computation of the droplet normalized surface energy (with respect to the radius of the cylinder R_C and the difference between the solid–liquid and the solid surface tension $\gamma_{(sl-s)}$) as a function of the volume (V_{drop}) for configurations on the top (red line) and on the side (blue line) of a cylindrical NW. The simulations were performed through the finite-element method based software Surface Evolver [36] with a contact angle of 43° on both the side and the top facets. (b)–(g) Illustrations of the equilibrium pinned droplet shape at different values of volume. The different volume values are indicated in the plot of normalized energy versus volume. The increasing volume produces an increase of the contact angle θ due to the pinning effect, as reported for each condition.

influence can be neglected. Regarding the wetting on the side facets, the droplet is not pinned nor influenced by the presence of the edges. It is therefore reasonable to simplify the shape by a cylinder. The chosen material system is liquid indium on InAs so that we can compare the theoretical/numerical results with our experiments.

To analyze the wetting behavior and stability of sessile droplets on top of a cylinder, we have used the modeling program Surface Evolver [36]. We have computed the surface energies of a sessile droplet as a function of its volume. We have analyzed three different configurations of the droplet: on the NW tip, half-way between the top and the side, and on the side of the NW. The half-way configuration is unstable for a cylindrical NW under the assumption of a perfectly flat tip. The results can be found in the supporting information (SI) is available online at stacks.iop.org/NANO/30/285604/mmedia. As input data of the material system, the computations use the experimental equilibrium contact angle of In on InAs, as measured on flat InAs by scanning electron micrographs (SEM). Surface Evolver uses this contact angle, a specified volume and contact constraints to iteratively modify the surface towards the shape of minimum surface energy.

Figure 2(a) illustrates the volume dependency of the surface energy associated with the equilibrium condition of the sessile droplet. According to Laplace's law, the surface energy is proportional to the mean curvature of the shape of the droplet and to its volume. The energy values reported have been normalized by the volume of the droplet, V_{drop} , the difference between the solid–liquid tension and the solid surface tension γ_{sl-l} and the radius of the cylinder, R_C . The red and blue points represent the configuration in which the droplet is respectively on the NW tip or side facet. Starting for the configuration on the NW tip, we see that the surface energy does not vary for increasing volume until pinning. As soon as the droplet is pinned at the edge of the NW tip, the surface energy starts to increase. The surface energy evolution of the droplet on the NW side facet is more gradually increasing. This is due to the particular variation of the shape

of the droplet on the cylindrical side facets. Our calculations show that at a certain volume (between points e and f in figure 2(a)) the droplet on the NW tip becomes less stable than on the side facet. This corresponds to the turning point of its stability and indicates the maximum value of the apparent contact angle. Overall, pinning of the droplet at the edge of the NW tip allows for the engineering of the contact angle from approximately 43° – 100° . This is a remarkably large range of variation.

So far, we have explained the interplay between the droplet volume, the contact angle and the stability of the droplet on the NW tip. Still, some open questions arise with respect to the nature of the TPL and the pinning line. We also have considered that the droplet pins on an atomically sharp corner at the NW edge. Still, chances are that this corner is not atomically sharp and that it exhibits a certain curvature as it is for the edges of the NW cross-section [37, 38].

Figure 3 illustrates the relationship between the advancing triple line, the apparent contact angle, the equilibrium angle, and the orientation of neighboring surfaces. One of the points we want to make is that the macroscopically observed contact angle θ' may differ from the Young contact angle θ_y on a planar substrate. Eventually, the contact angle may continue to be the Young contact angle θ_y locally, if the solid at the TPL deforms gradually and/or if the corner is not atomically sharp. In the left part of figures 3(a) and (b) we depict the variation in the observed contact angle for a droplet moving from the top to the side surface. We differentiate the cases in which the corner between the two surfaces is atomically sharp or round. The latter could also correspond to the case in which the solid at the TPL is deformable. We define the apparent angle θ' as the one measured with respect to the horizontal plane. θ' varies in a step-wise manner or continuously depending on whether the solid at the TPL is atomically sharp or smooth. In the case of smooth corners, θ' depends on the continuous change of inclination as the TPL traverses the rounded corner. From a macroscopic point of view, the abrupt increase of the droplet volume translates into

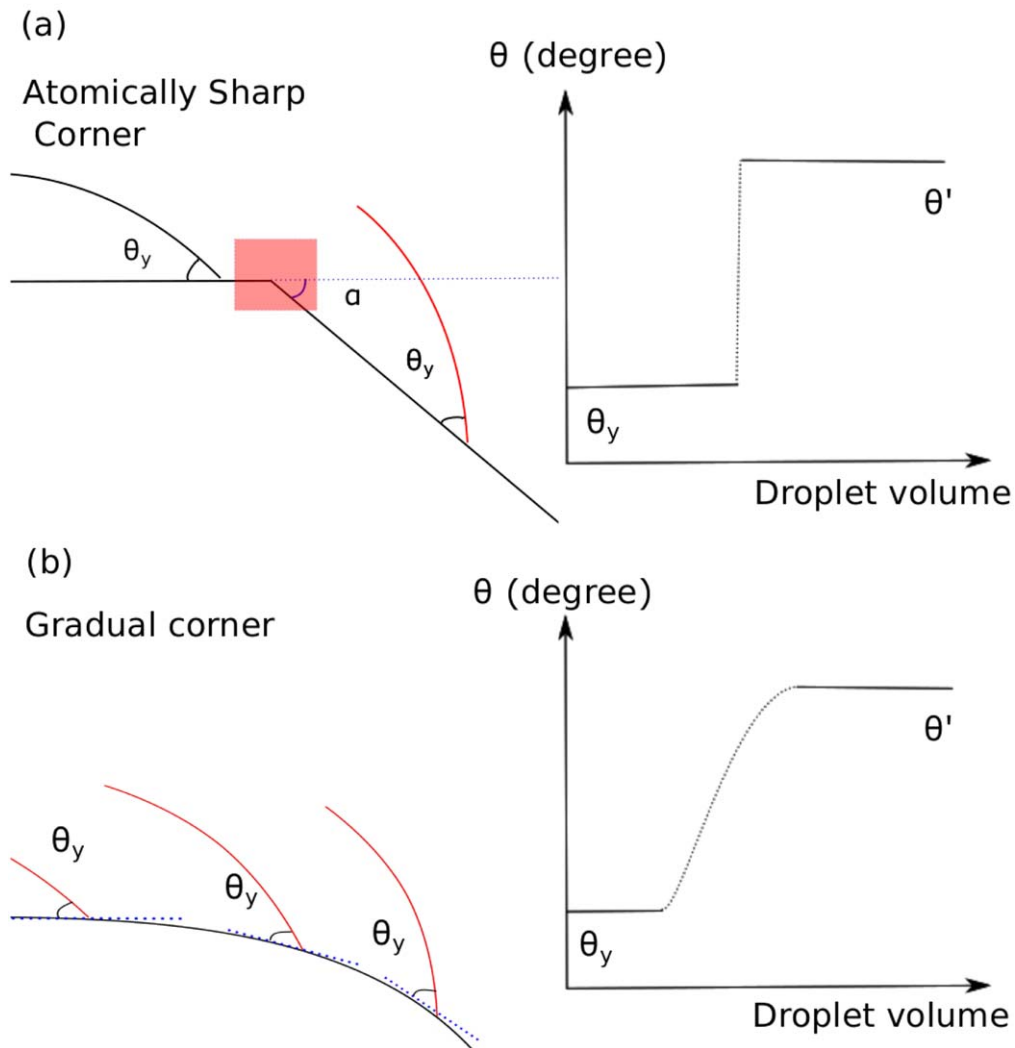


Figure 3. Representative sketch illustrating the behavior of the apparent angle of sessile droplets. The effect of neighboring facets is illustrated for both an atomically sharp (a) and a smooth corner (b). In the first case, the bistability condition of the apparent angle is due to the advancing of the TPL. The rapid change of apparent angle with triple line position in the microscopic illustration results in a seemingly discontinuous change in the macroscopic view.

the appearance of two preferential apparent angles (bistability condition). The first one corresponds to the equilibrium Young's angle θ_y , while the second one is the critical angle $\theta_{crit} = \theta_y + \alpha$, with α being the inclination of the neighboring facet, assuming Young's angle equal to θ_y also on the inclined surface. From a microscopic point of view, the departure of the triple line from the sharp corner needs a finite increase in the droplet volume and the deformation of the solid around the corner, which results in a continuous modification of the apparent angle until the value of the critical angle is reached. This defines the range of available pinned (apparent) angles as $\theta_y < \theta_{pin} < (\theta_y + \alpha)$ and consequently the related range of pinned volume.

We come back now to the detailed discussion of the Young–Dupré equation, to further discuss the force equilibrium at the TPL and its role in determining the droplet stability. In particular, we consider 2 main cases, depicted in figure 4:

Case 1 (C1): The triple line is constrained to a microscopically smooth planar solid-interface as shown in inset a of figure 4 (i.e. atoms in solid are immobile). The position of the triple line changes with droplet volume. The equilibrium at the triple junction requires that contact angles obey the Young–Dupré equation (1).

The previous equations are often derived also as a balance of forces at the TPL and thus as a vectorial equilibrium [39]. The Young–Dupré equation is a necessary boundary condition to a minimal surface problem. That is, it holds for any minimizing surface which has contact lines on smooth surfaces regardless if the surface is a global or local minimum. Furthermore, the condition can be satisfied with the motion of only tens of atoms whereas surface minimization requires long-range transport: it is impossible to stabilize a non-equilibrium contact angle on a smooth surface [35]. In the Young–Dupré equation, only the capillary forces in the plane of the solid sum to zero. The vertical capillary forces are

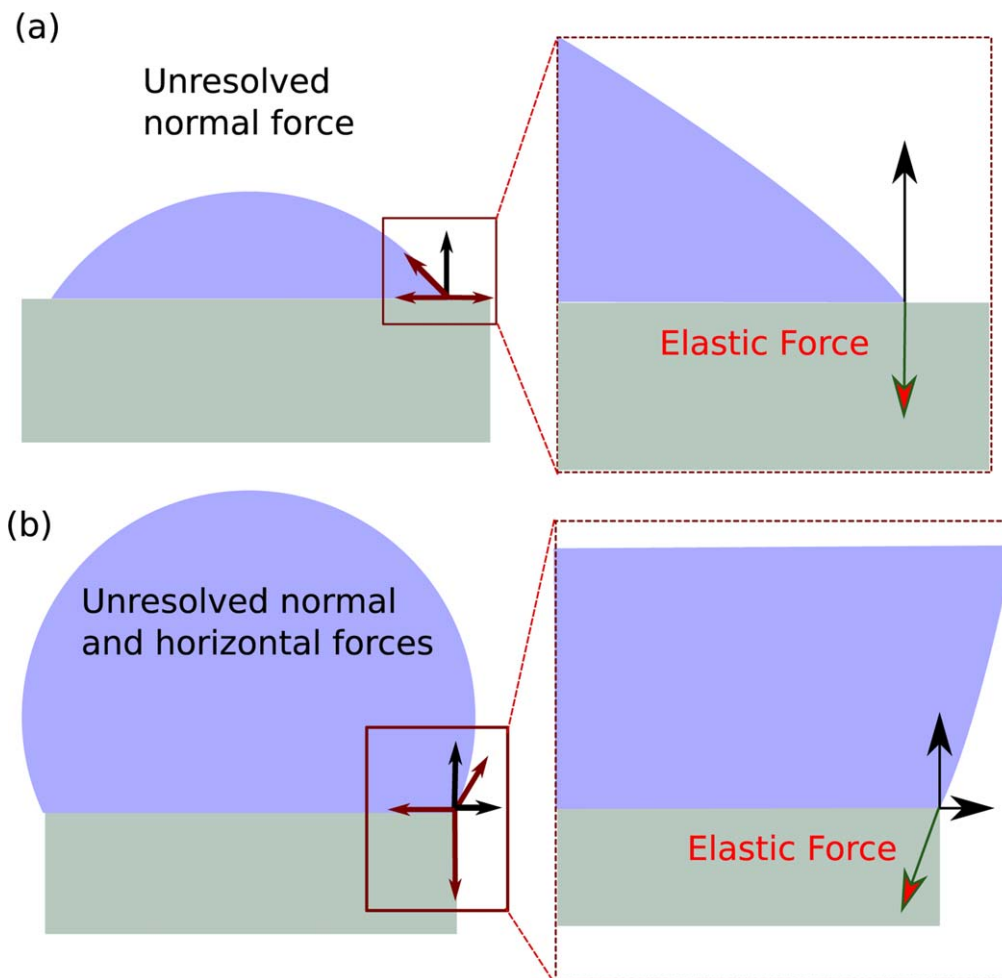


Figure 4. Sketch representing the 2 cases in which the Young equation does not ensure the balance of forces. (a) This happens already to the vertical component of the forces applied on the droplet, which is balanced by the elastic stresses of the solid. (b) When the triple junction is at the corner, the imbalance of the forces happens both in the vertical and in the horizontal plane, allowing the stress field of the solid to rotate at the corner.

depicted in the sketch (a) in figure 4 in the case the atoms on the surface of the solid are immobile. Because the forces must always sum to zero everywhere across the contact surface, the capillary forces are balanced by elastic stresses resolved onto the solid surface. If the solid were elastically compliant (i.e. a thin substrate), it would bend (and thereby reduce the total elastic energy). As an extension of this case, the solid–liquid and/or the vapor–solid interface may deform by diffusion in the solid, such as that observed by Tomsia *et al* [40]. In this condition, the equation (1) is adjusted to account for the deformation of the solid.

Case 2 (C2): The TPL intersects a solid edge and the atoms of the solid are immobile, as depicted in figure 4(b). In this case, the direction of the resolved singular elastic force in the vicinity of the TPL is no longer constrained to be vertical and the stress field can rotate at the edge. The TPL translational degree of freedom is removed and replaced by a variable apparent angle (i.e. the apparent angle increases as the droplet volume increases). The corner will continue to pin the triple line until the condition for capillary force-balance is satisfied on the adjacent solid surface—equivalently, the equilibrium Young angle is satisfied on the adjacent surface.

As discussed above, the range of stable angles can be treated as the limiting case as the solid interface’s radius of curvature goes to zero.

As an extension to case C2, we can consider also the case of rough surfaces. Microscopic corners and edges pin the contact line and the apparent angle can vary until the TPL unpins. Roughness adds further complexities as pinning can also occur at corners where three or more edges intersect and the direction of the edges needs not be parallel to the (macroscopic) TPL. Nevertheless, the elastic/capillary force balance always applies when geometric features are resolved at the microscopic scale. The difference between microscopic and apparent (macroscopic) geometric features gives rise to Cassie phenomena [41].

In summary, so far we have elucidated the volume dependency of the equilibrium condition of sessile droplets wetting the tip and the sidewalls of cylindrical NWs. We have then explained how the pinning of the droplets at the NW edge can account for a large variation of the observed contact angle from the equilibrium condition at a flat surface. Finally, we have proposed that the finite-size nature of the edges may also explain part of the variability in available contact angles.

Experimental results: indium droplets on InAs NWs

We turn now to the experimental investigation of liquid droplets on NW tips. We consider the system formed by an In droplet on an InAs NW. The InAs NWs were obtained in a catalyst-free manner by self-assembly on a GaAs(111) B substrates as in [24].

These NWs typically exhibit a flat tip. By annealing the NWs in vacuum after growth at 530 °C it is possible to incongruently evaporate the arsenic from the NW tip, forming a pure In droplet. The experiments show that, with increasing the annealing time, the droplets increase their volume and move from the NW tip to the side facets, wetting simultaneously two {110} facets. In a related publication, we have shown that these droplets can be further used to nucleate the growth of InAs in a second step in the form of branches perpendicular to the direction of the primary NW [24, 42].

Here, we analyze the evolution of the shape and stability of the droplets as a function of their volume, gauged by the annealing time. Spherical cap droplet shapes have been treated previously [26, 32]. To the best of our knowledge, the transition of the droplets to lower energy shapes and/or the evolution of TPL pinning and depinning have not been analyzed for pure Indium wetting InAs NWs.

Figures 5(a)–(e) shows the SEM of the InAs NW tips for five different annealing times: 3, 5, 7, 10 and 15 min. Here we consider the evolution of the droplets *ex situ*. Even if previous studies show that this is a reasonable assumption [43], we still remind the reader that contact angle values may be affected from the modification of the environment. We observe three different configurations of the droplets: at the tip, transitioning to the side facet and on the side facets. For the three observed configurations, we have measured the apparent contact angle, defined by the angle between the apparent L–S interface and the droplet tangent at the TPL. A histogram depicting the distribution of contact angles obtained for the different annealing times is shown in figure 5(f). The reported values have been determined using the Carl Zeiss Microscopy, LLC—AxioVision Software. The measurements are affected by both picture resolution uncertainty and human mistake. A statistics of the uncertainty performed on different SEM pictures show that the statistical variation of the measurement ranges from $\pm 3^\circ$ to $\pm 8^\circ$, depending on the resolution of the picture. After 3 min of annealing, some InAs NWs have small In droplets on their top surface. The measured apparent angle is 43° on average. This is consistent with the known equilibrium contact angle of indium droplet on (111)B InAs (i.e. determined by the Young–Dupré equation). As annealing proceeds and the droplet volume increases, the liquid spreads to the edges of the NW tip. As soon as the droplet pins at the edge, the angle increases. At 5 and 7 min, the average apparent angle is respectively 100° and 115° . We note that the angle distribution has become significantly broader, from few degrees to few tens of degrees. After 7 min annealing, the liquid droplets begin to relocate from the NW tip to the sides. We find an intermediate configuration in which the droplet is in the transition from the tip to the side

facet, which we denominated as half-way configuration. Clearly, in this case, the liquid–solid interface has been tilted. The fraction of droplets on the side facets increases with time and reaches a yield of 100% after 15 min. The distribution of the contact angle on the NW side facets is also quite broad. Half-way droplets have an even wider range of apparent angles. We believe this range results from uncertainty in the surface inclination, but also from the variation in the pinning at the sharp edge as it will be further elucidated here below. In figure 5(f), the graphic insets represent the three observed droplet configurations. The contact geometry is illustrated assuming that the NW is cylindrical, although it is known that (111)B InAs NW cross-sections are hexagonal [14, 44].

We turn now to the analysis of the droplets in the half-way configuration. In particular, we look at the shape of the liquid–solid interface. The indium droplet was removed by immersing the NWs for 10 min in isopropyl alcohol (IPA). Figure 6 shows representative SEM images of the tip of these NWs after removal of the droplet. This sample corresponds to the NWs annealed for 7 min. Numerous NWs terminated with truncated facets were observed. These truncated facets have 2 main inclinations with respect to the top surface; 67° and 52° . These facet inclinations would coincide respectively with the orientation of (111) and (311) surfaces. The formation of these slanted facets has been previously predicted for both self-catalyzed and gold-assisted III–V NWs growth techniques [3, 25, 32]. Their presence was also predicted by molecular dynamics simulations on the equilibrium of liquid–solid interfaces for VLS growth of NWs [45].

The presence of two preferential inclinations translate also in the observation of two preferential apparent angles. As shown in figure 5(f) the most probable apparent angles are 100° for smaller (5 min annealing) and 115° for larger droplets (7 min annealing). Smaller droplets tend to be located on the lowest inclination (52°) surface; while for larger droplets, the TPL line intersects the surfaces with inclination 67° , on their way to wet the vertical NW side facets. We thus propose that in the transition of the droplet from the NW tip to the side facets, the NW edge disappears to form new slanted facets with rising inclination when the volume increases. This observation confirms the non-static nature of the NW edges and the interaction/exchange of the material with the droplet. These results highlight that measuring the apparent contact angle and analyzing it with the Young–Dupré equation can lead to a misinterpretation. This is particularly evident in cases where the TPL contacts a surface with rapidly varying inclination. As opposed to the Young contact angle, the apparent angle of droplets on NW tips is measured with respect to the ideally perfectly horizontal top facet of the NWs. It is clear that the apparent angle is not necessarily related to the surface energy of the top facet of the NWs. As a consequence, relating the apparent angle to the Young–Dupré equation should necessarily lead to the misinterpretation of the energetics of the system (i.e. incorrectly assuming that neighboring facets have the same energy or that the apparent angle is not measured with respect to the correct surface).

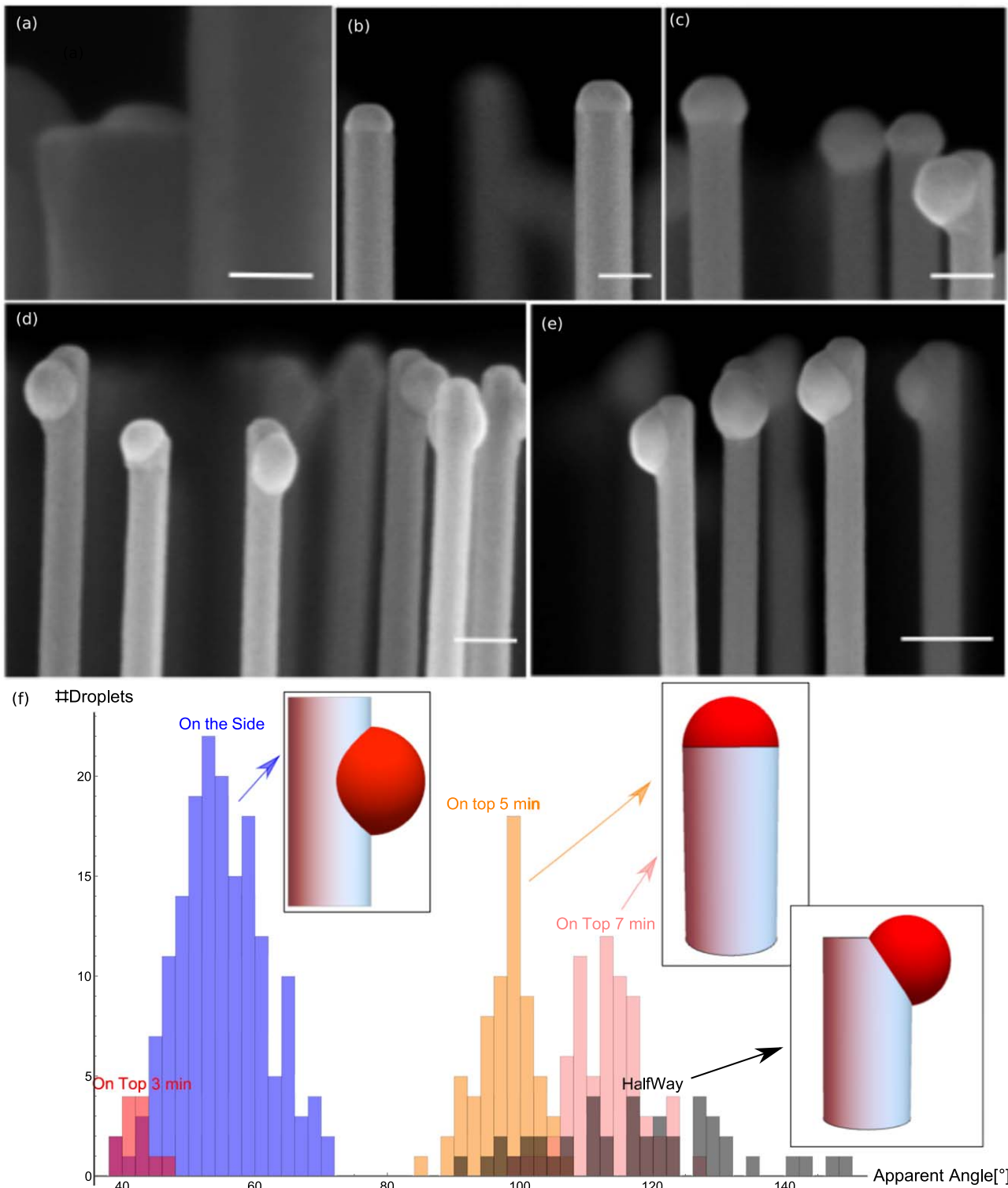


Figure 5. Stability of the In droplets on top of InAs NWs. (a)–(e) Scanning electron micrographs of the InAs NW tips after the annealing process. The annealing times were (a) 3 min, (b) 5 min, (c) 7 min, (d) 10 min and (e) 15 min. The scale bars represent 20 nm in (a) and 100 nm for the other images. (f) Distribution of the apparent angles for different annealing times and for the three different configurations: top of the NW, on the side facets and half-way. These configurations are shown schematically in the respective insets. The values of apparent angle of half-way (black) and side (blue) positioned droplets obtained with 7, 10 and 15 min annealing are similarly scattered and plotted together. The apparent angle of the liquid droplet on the top of the NW increases with increasing annealing time, and thus with the In volume. The annealing process introduces new facets onto the previously flat liquid–vapor interface.

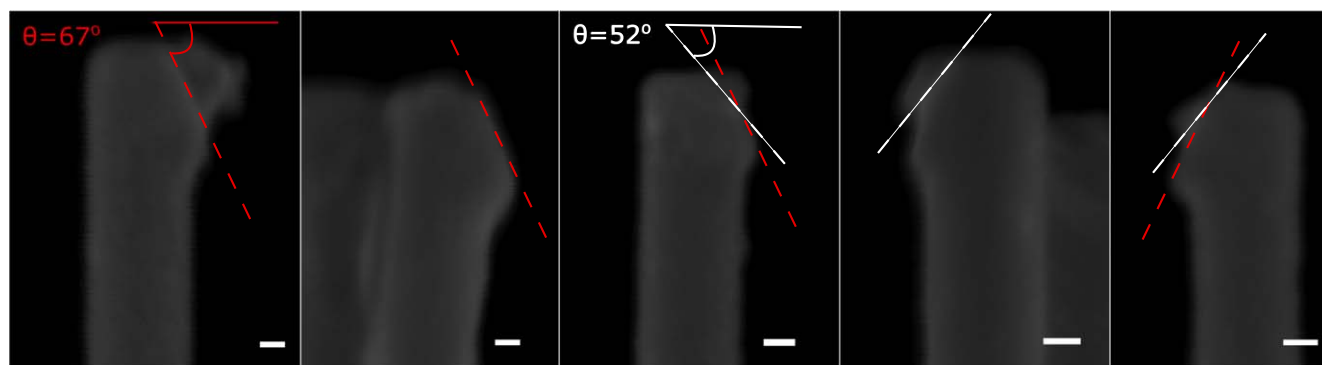


Figure 6. SEM pictures of the tip of InAs NWs grown on GaAs(111)B after a 7 min annealing procedure and removal of the Indium droplets. The inclinations of the slanted facets formed during arsenic evaporation are shown are of 67° and 52° for red and white dashed lines respectively. The scale bars correspond to 20 nm.

Conclusions

In conclusion, we have performed numerical simulations to show that the stability and morphology of a liquid droplet on a NW tip depend on three main factors: its volume relative to the dimensions of a NW, the presence of slanted facets and the equilibrium contact angle. As volume increases, the droplet is pinned by the NW edges that separate the NW side surfaces from its top surfaces. The apparent contact angle increases with the droplet volume up to a critical volume, after which the TPL unpins from the edges to relocate on the side of the NW. Our simulations are supported with experimental observations for indium droplets on InAs NWs. Finally, we also experimentally present the formation of slanted facets in the transition from the NW tip to the side facets and discuss their implications on contact angle measurements and interpretation.

Acknowledgments

Authors thank funding from SNSF via project nr 200021_169908, IZLRZ2_163861 and the NCCR QSIT, as well as H2020 program through project Indeed and Limquet.

ORCID iDs

Anna Fontcuberta i Morral  <https://orcid.org/0000-0002-5070-2196>

References

- [1] Ionescu A M and Riel H 2011 *Nature* **479** 329
- [2] Cartwright J 2011 *Nature News* **2011** 274
- [3] Krogstrup P, Jørgensen H I, Heiss M, Demichel O, Holm J V, Aagesen M, Nygård J and Fontcuberta i Morral A 2013 *Nat. Photon.* **7** 306
- [4] Dimroth F and Kurtz S 2007 *MRS Bull.* **32** 230
- [5] Plissard S *et al* 2013 *Nat. Nanotechnol.* **8** 859
- [6] Kammhuber J *et al* 2017 *Nat. Commun.* **8** 478
- [7] Alicea J, Oreg Y, Refael G, von Oppen F and Fisher M P A 2011 *Nat. Phys.* **7** 412
- [8] Kim W, Dubrovskii V G, Vukajlovic-Plestina J, Tütüncüoğlu G, Francaviglia L, Güniat L, Potts H, Friedl M, Leran J-B and Morral A F i 2018 *Nano Lett.* **18** 49–57
- [9] Mårtensson T, Carlberg P, Borgström M, Montelius L, Seifert W and Samuelson L 2004 *Nano Lett.* **4** 699
- [10] Pierret A, Hocevar M, Diedenhofen S L, Algra R E, Vlieg E, Timmering E C, Verschuuren M A, Immink G W G, Verheijen M A and Bakkers E P A M 2010 *Nanotechnology* **21** 065305
- [11] Wu Z H, Mei X Y, Kim D, Blumin M and Ruda H E 2002 *Appl. Phys. Lett.* **81** 5177
- [12] Zamani M *et al* 2018 *Nanoscale* **10** 17080
- [13] Fonseka H A, Caroff P, Wong-Leung J, Ameruddin A S, Tan H H and Jagadish C 2014 *ACS Nano* **8** 6945
- [14] Kobl Müller G, Hertenberger S, Vizbaras K, Bichler M, Bao F, Zhang J-P and Abstreiter G 2010 *Nanotechnology* **21** 365602
- [15] Jabeen F, Grillo V, Rubini S and Martelli F 2008 *Nanotechnology* **19** 275711
- [16] Koivusalo E, Hakkarainen T and Guina M 2017 *Nanoscale Res. Lett.* **12** 192
- [17] Givargizov E I 1975 *J. Cryst. Growth* **31** 20
- [18] Yazawa M, Koguchi M, Muto A, Ozawa M and Hiruma K 1992 *Appl. Phys. Lett.* **61** 2051
- [19] Glas F, Harmand J-C and Patriarche G 2007 *Phys. Rev. Lett.* **99** 146101
- [20] Wagner R S and Ellis W C 1964 *Appl. Phys. Lett.* **4** 89
- [21] Binkerd E F and Kolaril O E 1975 *Pergamon Press* **13** 655–61
- [22] Matteini F, Tütüncüoğlu G, Potts H, Jabeen F and Fontcuberta i Morral A 2015 *Cryst. Growth Des.* **15** 3105
- [23] Yuan X, Caroff P, Wong-Leung J, Fu L, Tan H H and Jagadish C 2015 *Adv. Mater.* **27** 6096–103
- [24] Potts H, Morgan N P, Tütüncüoğlu G, Friedl M and Fontcuberta i Morral A 2017 *Nanotechnology* **28** 054001
- [25] Jacobsson D, Panciera F, Tersoff J, Reuter M C, Lehmann S, Hofmann S, Dick K A and Ross F M 2016 *Nature* **531** 317
- [26] Tornberg M, Dick K A and Lehmann S 2017 *J. Phys. Chem. C* **121** 21678
- [27] O'Dowd B J *et al* 2014 *J. Appl. Phys.* **116** 063509
- [28] Schmidt V, Wittemann J V, Senz S and Gösele U 2009 *Adv. Mater.* **21** 2681
- [29] Krogstrup P, Curio S, Johnson E, Aagesen M, Nygård J and Chatain D 2011 *Phys. Rev. Lett.* **106** 125505
- [30] Kolibal M, Vystavěl T, Varga P and Šikola T 2014 *Nano Lett.* **14** 1756
- [31] Nebol'sin V A and Shchetinin A A 2003 *Inorg. Mater.* **39** 899
- [32] Dubrovskii V G 2017 *Cryst. Growth Des.* **17** 2544–8

- [33] Zannier V, Ercolani D, Gomes U P, David J, Gemmi M, Dubrovskii V G and Sorba L 2016 *Nano Lett.* **16** 7183
- [34] Fang G and Amirfazli A 2012 *Langmuir* **28** 9421
- [35] Carter W 1988 *Acta Metall.* **36** 2283
- [36] Brakke K A 1992 *Exp. Math.* **1** 141
- [37] Heiss M *et al* 2013 *Nat. Mater.* **12** 439
- [38] Steinke L, Cantwell P, Stach E, Schuh D, Fontcuberta i Morral A, Bichler M, Abstreiter G and Grayson M 2013 *Phys. Rev. B* **87** 165428
- [39] Young T 1805 *Phil. Trans. R. Soc.* **95** 6
- [40] Saiz E, Tomsia A P and Cannon R M 1998 *Acta Mater.* **7** 2349
- [41] Cassie A B D and Baxter S 1944 *Trans. Faraday Soc.* **40** 546
- [42] Koivusalo E S, Hakkarainen T V, Galeti H V A, Gobato Y G, Dubrovskii V G and Guina M D 2017 *Nano Lett.* **17** 5350–5
- [43] Yuan X, Caroff P, Wong Leung J, Fu L, Tan H H and Jagadish C 2015 *Adv. Mater.* **27** 6096
- [44] Johansson J, Karlsson L S, Svensson C P T, Mårtensson T, Wacaser B A, Deppert K, Samuelson L and Seifert W 2006 *Nat. Mater.* **5** 574
- [45] Frolov T, Carter W C and Asta M 2014 *Nano Lett.* **14** 3577